

## Preparation of lithium-ion battery anode materials from graphitized spent carbon cathode derived from aluminum electrolysis

Zhihao Zheng, Mingzhuang Xie, Guoqing Yu, Zegang Wu, Jingjing Zhong, Yi Wang, Hongliang Zhao, and Fengqin Liu

Cite this article as:

Zhihao Zheng, Mingzhuang Xie, Guoqing Yu, Zegang Wu, Jingjing Zhong, Yi Wang, Hongliang Zhao, and Fengqin Liu, Preparation of lithium-ion battery anode materials from graphitized spent carbon cathode derived from aluminum electrolysis, *Int. J. Miner. Metall. Mater.*, 31(2024), No. 11, pp. 2466-2475. <https://doi.org/10.1007/s12613-024-2866-z>

View the article online at [SpringerLink](#) or [IJMMM Webpage](#).

### Articles you may be interested in

Qi Wang, Yue-yong Du, Yan-qing Lai, Fang-yang Liu, Liang-xing Jiang, and Ming Jia, [Three-dimensional antimony sulfide anode with carbon nanotube interphase modified for lithium-ion batteries](#), *Int. J. Miner. Metall. Mater.*, 28(2021), No. 10, pp. 1629-1635. <https://doi.org/10.1007/s12613-021-2249-7>

Cheng Yang, Jia-liang Zhang, Qian-kun Jing, Yu-bo Liu, Yong-qiang Chen, and Cheng-yan Wang, [Recovery and regeneration of  \$\text{LiFePO}\_4\$  from spent lithium-ion batteries via a novel pretreatment process](#), *Int. J. Miner. Metall. Mater.*, 28(2021), No. 9, pp. 1478-1487. <https://doi.org/10.1007/s12613-020-2137-6>

Liu-ye Sun, Bo-rui Liu, Tong Wu, Guan-ge Wang, Qing Huang, Yue-feng Su, and Feng Wu, [Hydrometallurgical recycling of valuable metals from spent lithium-ion batteries by reductive leaching with stannous chloride](#), *Int. J. Miner. Metall. Mater.*, 28(2021), No. 6, pp. 991-1000. <https://doi.org/10.1007/s12613-020-2115-z>

Qiao-kun Du, Qing-xia Wu, Hong-xun Wang, Xiang-juan Meng, Ze-kai Ji, Shu Zhao, Wei-wei Zhu, Chuang Liu, Min Ling, and Cheng-du Liang, [Carbon dot-modified silicon nanoparticles for lithium-ion batteries](#), *Int. J. Miner. Metall. Mater.*, 28(2021), No. 10, pp. 1603-1610. <https://doi.org/10.1007/s12613-020-2247-1>

Zhi-yuan Feng, Wen-jie Peng, Zhi-xing Wang, Hua-jun Guo, Xin-hai Li, Guo-chun Yan, and Jie-xi Wang, [Review of silicon-based alloys for lithium-ion battery anodes](#), *Int. J. Miner. Metall. Mater.*, 28(2021), No. 10, pp. 1549-1564. <https://doi.org/10.1007/s12613-021-2335-x>

Kai-lin Cheng, Dao-bin Mu, Bo-rong Wu, Lei Wang, Ying Jiang, and Rui Wang, [Electrochemical performance of a nickel-rich  \$\text{LiNi}\_{0.6}\text{Co}\_{0.2}\text{Mn}\_{0.2}\text{O}\_2\$  cathode material for lithium-ion batteries under different cut-off voltages](#), *Int. J. Miner. Metall. Mater.*, 24(2017), No. 3, pp. 342-351. <https://doi.org/10.1007/s12613-017-1413-6>





IJMMM WeChat



QQ author group

# Preparation of lithium-ion battery anode materials from graphitized spent carbon cathode derived from aluminum electrolysis

Zhihao Zheng<sup>1,2)</sup>, Mingzhuang Xie<sup>1,2)</sup>, Guoqing Yu<sup>1,2)</sup>, Zegang Wu<sup>1,2)</sup>, Jingjing Zhong<sup>1,2)</sup>, Yi Wang<sup>1,2)</sup>, Hongliang Zhao<sup>1,2)</sup>,, and Fengqin Liu<sup>1,2)</sup>,

1) State Key Laboratory of Advanced Metallurgy, University of Science and Technology Beijing, Beijing 100083, China

2) School of Metallurgical and Ecological Engineering, University of Science and Technology Beijing, Beijing 100083, China

(Received: 13 November 2023; revised: 20 February 2024; accepted: 26 February 2024)

**Abstract:** Graphitized spent carbon cathode (SCC) is a hazardous solid waste generated in the aluminum electrolysis process. In this study, a flotation–acid leaching process is proposed for the purification of graphitized SCC, and the use of the purified SCC as an anode material for lithium-ion batteries is explored. The flotation and acid leaching processes were separately optimized through one-way experiments. The maximum SCC carbon content (93wt%) was achieved at a 90% proportion of –200-mesh flotation particle size, a slurry concentration of 10wt%, a rotation speed of 1600 r/min, and an inflatable capacity of 0.2 m<sup>3</sup>/h (referred to as FSCC). In the subsequent acid leaching process, the SCC carbon content reached 99.58wt% at a leaching concentration of 5 mol/L, a leaching time of 100 min, a leaching temperature of 85°C, and an HCl/FSCC volume ratio of 5:1. The purified graphitized SCC (referred to as FSCC-CL) was utilized as an anode material, and it exhibited an initial capacity of 348.2 mAh/g at 0.1 C and a reversible capacity of 347.8 mAh/g after 100 cycles. Moreover, compared with commercial graphite, FSCC-CL exhibited better reversibility and cycle stability. Thus, purified SCC is an important candidate for anode material, and the flotation–acid leaching purification method is suitable for the resourceful recycling of SCC.

**Keywords:** graphitized spent carbon cathode; hazardous solid waste; flotation; acid leaching; lithium-ion batteries

## 1. Introduction

Aluminum is an indispensable non-ferrous metal with extensive applications; thus, the production of electrolytic aluminum has increased. In 2022, the global electrolytic aluminum production capacity exceeded 65 million metric tons, of which China's production accounted for over 50%. Alumina molten salt electrolysis is the most mature process of aluminum smelting. The alumina is first dissolved in cryolite through electrolysis to obtain primary aluminum. In the electrolysis process, the cathode carbon in the cell is constantly exposed to alumina liquid, which leads to high-temperature electrolyte infiltration erosion [1]. Thus, aluminum cathode cells have a typical operating life of six to eight years. Spent carbon cathode (SCC), produced at a rate of 20–30 kg per t Al during aluminum electrolysis, is considered a hazardous waste, and about 1 million metric tons were generated in 2022. A large amount of waste cathode charcoal briquettes presents a significant risk for environmental pollution owing to uncontrolled accumulation without suitable disposal methods [2].

Considering the large amount of fluoride and small amount of cyanide present in spent cathode charcoal briquettes [3], SCC disposal has a significant environmental im-

pact. Studies have shown that the soluble F content in SCCs is approximately 2000–6000 mg/L, and the CN<sup>−</sup> content is approximately 10–40 mg/L, both of which are far above the safe emission standards (GB5085.3-2007). Therefore, the U.S. Environmental Protection Agency and the Ministry of Ecology and Environment of China have labeled the SCCs generated during the production of aluminum electrolysis as hazardous waste [4].

SCCs contain a large amount of graphitized carbon and fluoride and thus hold significant recycling value. Achieving efficient separation of carbon and electrolyte, transforming hazardous solid waste into general industrial solid waste, and realizing the resourceful use of valuable components are important research objectives in this field. To solve the environmental problems caused by SCCs and achieve the safe treatment and resource utilization of SCCs, several SCC purification and treatment methods have been explored. These approaches can be divided into thermal and wet processes, such as high-temperature roasting, alkali fusion, flotation, and chemical leaching [5–8]. While these methods can help obtain nontoxic SCCs and separate carbon and the electrolyte in a single removal method, they result in insufficient carbon purity and underutilization of carbon materials.

Considering that the graphitization degree of the carbon

 Corresponding authors: Hongliang Zhao E-mail: [zhaohl@ustb.edu.cn](mailto:zhaohl@ustb.edu.cn); Fengqin Liu E-mail: [liufq@ustb.edu.cn](mailto:liufq@ustb.edu.cn)

© University of Science and Technology Beijing 2024

materials can reach 80%–90% [9], recycled graphitized spent materials have the potential to be applied as lithium-ion anode materials. Graphite anode material plays an important role in the field of electronic products [10]. Yu *et al.* [11] proposed a short-process, high-temperature regeneration method to ensure that the treated graphite meets the basic requirements of the lithium-ion battery graphite negative electrode. Additionally, Tian's team [12–14] investigated the feasibility of extracting carbon from aluminum electrolysis-derived SCCs to obtain anode materials for lithium-ion batteries and enhance the recycling value of SCCs. First, the impurities in the SCCs were removed through a high-temperature graphitizing method at 2600°C, which increased the carbon content from 63.64wt% to 100wt%. As a lithium-ion anode, the material exhibited a specific capacity of 455.2 mAh/g for the first charging cycle and excellent reversible capacity compared with graphite [12]. Building on these findings, Tian's team proposed a lower-temperature roasting method to purify SCCs and assessed the feasibility of utilizing them as lithium-ion battery anodes [13]. The purified SCC achieved a carbon content of 97.22wt% at a temperature of 1600°C, a roasting time of 1 h, and a particle size of 200 mesh. The SCC maintained a capacity of 365.5 mAh/g over 100 cycles at 0.1 C, and exhibited a good reversible capacity. They [14] also proposed carbon recovery from SCCs through an alkali fusion method. The SCCs were roasted in a tube furnace at 450°C for 2 h, followed by leaching with hydrochloric acid and deionized water to recover carbon powder. The impurity content of the roasted SCC decreased by 31%. The initial charging specific capacity of the SCC as an anode material was 357.6 mAh/g at 0.1 C, and the rate capability at 1 C was 267.8 mAh/g. Thus, purification via alkali fusion improved the electrochemical performance of the SCC. The above process has been effectively applied to treat industrial solid wastes and SCCs to obtain anode materials for lithium-ion batteries.

Although high-temperature methods can effectively remove impurities in SCCs, they have high energy requirements and produce a large amount of toxic fluorine-containing exhaust gas. Therefore, this study proposes a combined flotation–acid leaching treatment process that does not require secondary heating, making the process more economical and energy-saving. Furthermore, the raw material is graphitized carbon, which has good structural properties and is more suitable for the preparation of anode materials. The effects of flotation and acid leaching processes on the carbon content and the impurity removal rate of SCC are experimentally investigated, and the electrochemical performance of purified SCC as lithium-ion batteries is explored. The technology also offers an effective approach for the clean recycling and high-value utilization of carbon-containing solid wastes.

## 2. Experimental

### 2.1. Materials

Graphitized SCC was provided by Zunyi Aluminum Co.,

Ltd., Guizhou, China and processed as follows: First, SCC was preliminarily crushed by a jaw crusher and oven-dried at 105°C for 12 h. After ball-milling and sieving with a –200 mesh (0.074 mm), the material was used for the subsequent purification tests. The elemental and phase compositions are shown in Table 1 and Fig. 1, respectively.

**Table 1.** Elemental composition and content of SCC wt%

C	F	Na	O	Al	Ca	Mg	Others
77.01	11.88	5.36	2.87	1.56	0.67	0.13	0.52

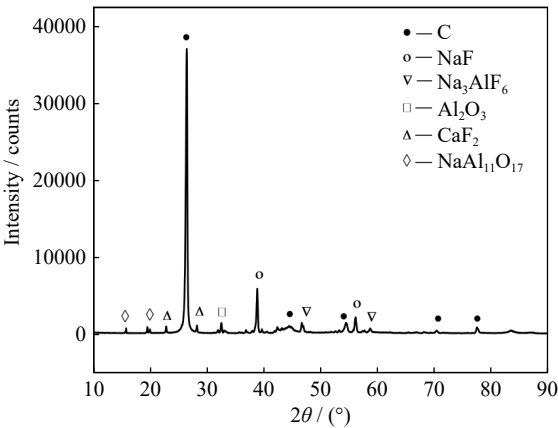


**Fig. 1.** XRD pattern of SCC.

### 2.2. Purification experiments

First, 200 g of SCC was weighed and placed in an XFD-1L flotation machine for preliminary flotation experiments (The Industrial analysis of the SCC as shown in Table 2). Single-factor experiments were conducted under varying conditions, including the percentage of particle size (–200 mesh), slurry concentration, spindle speed, and aerating volume. After the flotation test, the SCC referred to as FSCC, and the collected carbon material was oven-dried at 105°C for 8 h. Then, 10 g of the obtained material was weighed in a conical flask, and a certain amount of hydrochloric acid was added to remove impurities via acid leaching. The impacts of the leaching concentration, leaching temperature, leaching time, and HCl/FSCC volume ratio were studied. The experimental conditions are shown in Table 3. The leached carbon material was oven-dried at 105°C for 8 h, and the carbon content of the roasted residue was determined through the ash determination method.

**Table 2.** Industrial analysis of the SCC sample wt%

Moisture	Volatile matter	Ash	Fixed carbon
0.42	1.35	21.22	77.01

The carbon content of the roasting residue was used to characterize the extent of SCC purification as follows: The roasted residue was heated to 850°C in an air atmosphere in a muffle furnace and held for 3 h; then, the ash content (*A*, wt%) of the roasting residue was estimated as follows:

$$A = (m_2 - m_1) / m_0 \times 100\% \quad (1)$$

Table 3. Flotation and acid leaching condition experiment

Method	–200 mesh percentage / wt%	Slurry concentration / wt%	Rotation speed / (r·min <sup>–1</sup> )	Inflatable capacity / (m <sup>3</sup> ·h <sup>–1</sup> )
Flotation	50–100	5–30	1400–2200	0–0.4
Method	HCl concentration / (mol·L <sup>–1</sup> )	Leaching time / min	Leaching temperature / °C	HCl/FSCC volume ratio
Acid leaching	2–6	60–220	55–95	(2–15):1

where  $m_0$  (g) and  $m_1$  (g) are the weights of the carbon material and the ceramic boat before roasting, respectively, and  $m_2$  (g) is the weight of the ash and the ceramic boat after roasting.

2.3. Characterization

The phase compositions of the samples and impurities were characterized via X-ray diffraction (XRD, Rigaku3014, Cu K $\alpha$ ). The elemental composition and content were analyzed through X-ray fluorescence (XRF, XRF-1800, Shimadzu Corporation, Japan). The micromorphology and microstructure of the samples were analyzed via scanning electron microscopy (SEM, Quanta 250 FEG) and transmission electron microscopy (TEM, Tecnai G2 F20). The graphitization degree of the samples was investigated via Raman spectroscopy (LabRAM HR800, excitation wavelength 532 nm).

2.4. Electrochemical measurements

All of the electrochemical tests for the batteries were conducted in button cells (CR2025). The electrode slurry was prepared through the mixing of waste graphitized cathode carbon block-based carbon material, conductive agent (Super P), and binder (polyvinylidene difluoride, PVDF) at a mass ratio of 93:2:5. Then, appropriate amounts of dispersant and N-methyl pyrrolidone (NMP) were added and mixed well. After mixing, the slurry was coated on a copper foil, vacuum dried to remove the NMP, and then pressed into round electrode sheets with a tablet press. The cells were as-

sembled in a glove box in an argon atmosphere (both H<sub>2</sub>O content and O<sub>2</sub> content were less than 0.01 ppm). The button cell was assembled with the graphitized SCC tabs as the anode, lithium metal tabs as the cathode, polypropylene vinyl as the separator, and 1.0 mol/L LiPF<sub>6</sub>-EC/DEC (ethylene carbonate-diethyl carbonate) as the electrolyte. The constant-current charge/discharge test was performed using a LAND CT2001A battery tester at the voltage range of 0.01–3.00 V. Cyclic voltammetry (CV) measurements were conducted on a Shanghai Chenhua CHI660E electrochemical workstation at the voltage range of 0.01–3.00 V and a scanning rate of 0.1 mV/s. The electrochemical impedance test was also performed on a Shanghai Chenhua CHI660E electrochemical workstation at a test frequency of 10<sup>–2</sup>–10<sup>5</sup> Hz and an amplitude of 5 mV.

3. Results and discussion

3.1. Effect of flotation process on SCC carbon content

3.1.1. Effect of particle size

The optimal particle size was determined by considering different proportions of 200-mesh particles (50%, 60%, 70%, 80%, 90%, and 100%; 200 g each) as the raw material in the XFD-1L flotation tank flotation experiments (Fig. 2(a)). The results showed that owing to a more complete separation of the carbon and electrolyte, the flotation effect was better. Thus, a 90% proportion of –200-mesh particle size was optimal for flotation.

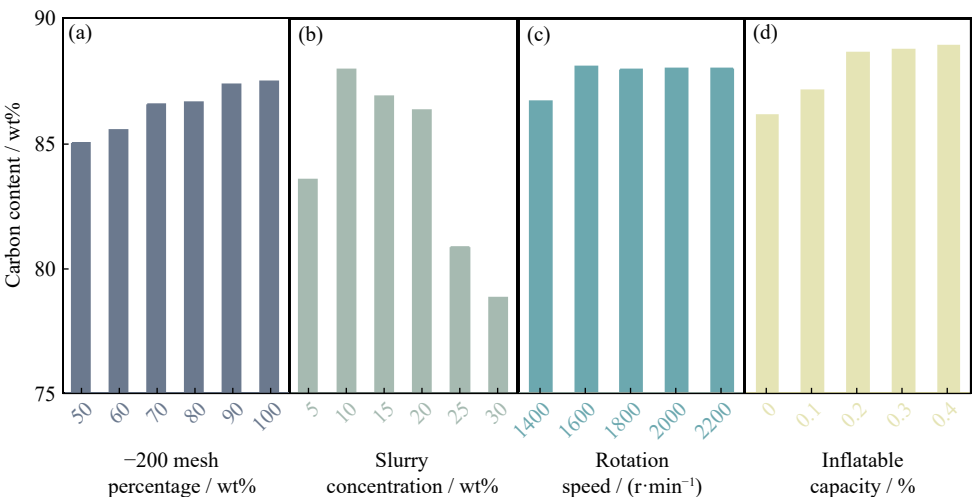


Fig. 2. Effects of particle size (a), slurry concentration (b), rotation speed (c), and inflatable capacity (d) on the SCC carbon content.

3.1.2. Effect of slurry concentration

To determine the optimum slurry concentration, flotation experiments were conducted using five slurry concentrations: 5wt%, 10wt%, 15wt%, 20wt%, 25wt%, and 30wt% (Fig. 2 (b)). The carbon content first increased and then decreased

with increasing concentration, because the mineral adhesion efficiency on the bubble was low at a low slurry concentration. As the slurry concentration increased, the aeration volume increased, the bubble loading capacity increased, and the sample particles had a greater chance of attaching to

bubbles. Under an excessively high slurry concentration, the slurry became thicker, and the bubble content increased. This increased the path impurity concentration, and mechanical entrapment was significant, reducing the carbon purity. Therefore, the optimum slurry concentration was 10wt%.

### 3.1.3. Effect of rotation speed

To determine the optimum rotation speed, 100 g of material was used to study the effects of five rotation speeds (1400, 1600, 1800, 2000, and 2200 r/min) on the flotation experiments (Fig. 2(c)). With the increase in the rotation speed, the carbon content first increased and then leveled off. With the increase in the spindle speed from 1400 to 1600 r/min, the carbon content increased from 86.69wt% to 88.09wt%, and at 2200 r/min, the carbon content gradually stabilized. Therefore, 1600 r/min was selected as the optimum rotation speed. The increasing rotational speed increased the mechanical force, enhancing the degree of dissociation between carbon and electrolyte [15]. Thus, the attachment efficiency of carbon to bubbles gradually increased, improving the purity of the toner.

### 3.1.4. Influence of inflatable capacity

To determine the optimal inflation capacity, 100 g of material was used to investigate the effect of five inflation capacities (0, 0.1, 0.2, 0.3, and 0.4 m<sup>3</sup>/h) on the flotation experiments (Fig. 2(d)). With the increase in the inflatable capacity, the carbon content increased and then leveled off. With the increase in the inflatable capacity from 0 to 0.2 m<sup>3</sup>/h, the carbon content increased from 86.14wt% to 88.63wt%. With the increase in the inflatable capacity to 0.3 and 0.4 m<sup>3</sup>/h, the carbon content gradually stabilized, with only a 0.10wt% and 0.27wt% increase, respectively. Therefore, 0.2 m<sup>3</sup>/h was selected as the optimum inflatable capacity. This indicates that as the inflatable capacity increased, the number of bubbles in the slurry increased, which improved the dispersion of carbon and the electrolyte in the slurry [16]. Additionally, the carbon–bubble contact continuously increased, which led to a gradual increase in the carbon content of the flotation concentrate.

### 3.1.5. Secondary flotation experiments

The entire flotation process is divided into primary and secondary flotation. The primary flotation ore is enriched with a large amount of carbonaceous material and contains a certain amount of electrolyte components. The flotation ore is then subjected to secondary flotation to further increase the carbon content. Under the optimal flotation conditions of 90% particle size at –200 mesh, 10wt% slurry concentration, 1600 r/min rotation speed, and 0.2 m<sup>3</sup>/h air inflation capacity, the carbon content of FSCC after secondary flotation reached 93wt% (Table 4).

**Table 4.** Carbon content after primary flotation and secondary flotation

Primary flotation	Secondary flotation
88	93

## 3.2. Effect of acid leaching process on FSCC carbon content

### 3.2.1. Effect of HCl concentration on FSCC carbon content

To determine the optimal leaching concentration, 10 g of material was used to conduct acid leaching experiments at concentrations of 2, 3, 4, 5, and 6 mol/L. With the increase in the leaching concentration, the carbon content of SCC first increased and then leveled off (Fig. 3(a)). With the gradual increase in the leaching concentration from 2 to 5 mol/L, the carbon content increased from 98.2wt% to 98.6wt%, owing to the increase in the hydrochloric acid leaching concentration, H<sup>+</sup> per unit volume, and the number of activated molecules. These factors promoted the chemical reaction and increased the rate of chemical reaction. With the further increase in the leaching concentration, the carbon content remained stable, and the H<sup>+</sup> concentration in the solution reached saturation. Further increase in the acid concentration had no significant effect on the reaction. Therefore, the leaching concentration of 5 mol/L was selected as the optimal leaching concentration.

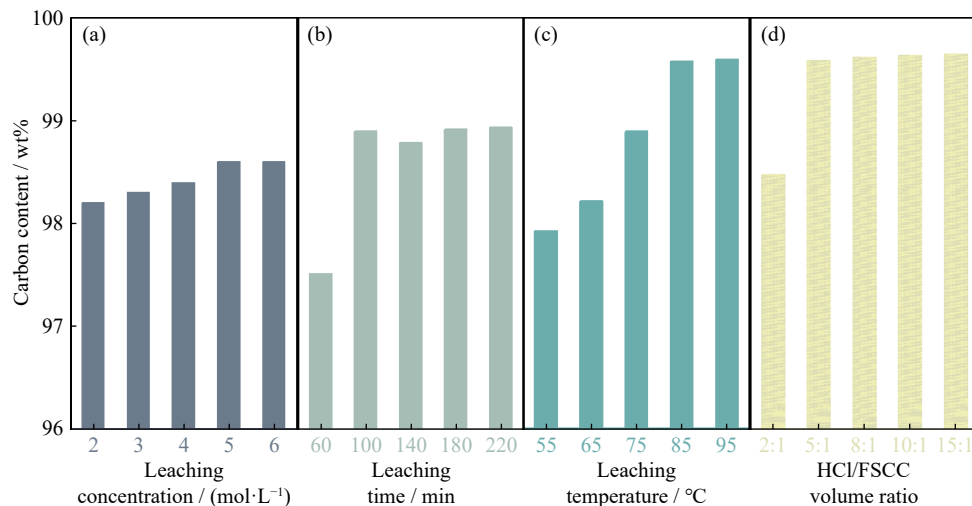


**Fig. 3.** Effects of HCl concentration (a), leaching time (b), leaching temperature (c), and HCl/FSCC volume ratio (d) on the FSCC carbon content.



### 3.2.2. Effect of leaching time on FSCC carbon content

To determine the optimal leaching time, 10 g of material was used for acid leaching experiments at 60, 100, 140, 180, and 220 min. With the increase in the leaching time from 60 to 100 min, the carbon content increased (Fig. 3(b)), because under sufficient reaction time, the hydrochloric acid solution could fully wet the flotation carbon residue and penetrate into the reaction kernel through the inter-layer pore structure of the carbon [17]. Thus, more non-carbon impurities can be dissolved, bringing the carbon content up to 98.57wt%. With further leaching, the carbon content no longer increased; therefore, 100 min was chosen as the optimal leaching time.

### 3.2.3. Effect of leaching temperature on FSCC carbon content

To determine the optimal temperature, 10 g of material was used for acid leaching experiments at temperatures of 55, 65, 75, 85, and 95°C. As shown in Fig. 3(c), with the increase in leaching temperature, the SCC content first increased and then gradually leveled off. With the gradual increase in the leaching temperature from 55 to 85°C, the carbon content increased from 97.92wt% to 99.57wt% because the rise in acid leaching temperature increased the internal energy of the molecules, accelerated the motion rate, and increased the entropy value of the system. With the continuous rise in temperature, the carbon content no longer changed. Therefore, the optimum temperature was chosen as 85°C.

### 3.2.4. Effect of HCl/FSCC volume ratio on FSCC carbon content

To determine the optimum liquid-to-solid ratio, 10 g of material was used for acid leaching experiments under liquid-to-solid ratios of 2:1, 5:1, 8:1, 10:1, and 15:1. The carbon content increased with the increase in the liquid-to-solid ratio (Fig. 3(d)). At a low liquid-to-solid ratio, the hydrochloric acid solution did not fully wet the raw material; thus, the chemical reaction could not effectively occur. The increase in the liquid-to-solid ratio was conducive to the diffusion of the solute molecules, which promoted the chemical reaction toward completion. However, the growth rate was very low after 5:1; thus, 5:1 was chosen as the optimal liquid-to-solid ratio, at a carbon content of 99.58wt%.

## 3.3. Structural characterization of purified graphitized SCC

To analyze the changes in impurities, composition, and morphology of SCC, FSCC, and purified graphitized SCC (FSCC-CL) before and after flotation–acid leaching, XRD was conducted (Fig. 4). The impurities in SCC mainly consisted of fluorides (NaF,  $\text{Na}_3\text{AlF}_6$ , and  $\text{CaF}_2$ ) and oxides ( $\text{Al}_2\text{O}_3$ ,  $\text{NaAl}_2\text{O}_7$ ).

Fig. 4. shows diffraction peaks of SCC, FSCC, and FSCC-CL near 26.48°, 42.35°, 44.52°, 54.50°, and 77.68°, which correspond to the characteristic (002), (100), (101), (004), and (110) reflections of graphite, respectively [18] (JCPDS No. 41-1487), typical of graphitic structures. However, the spectrum of FSCC-CL featured a significantly higher intensity of the (002) diffraction peak than the SCC and FSCC spectra and was without some weak impurity peaks.

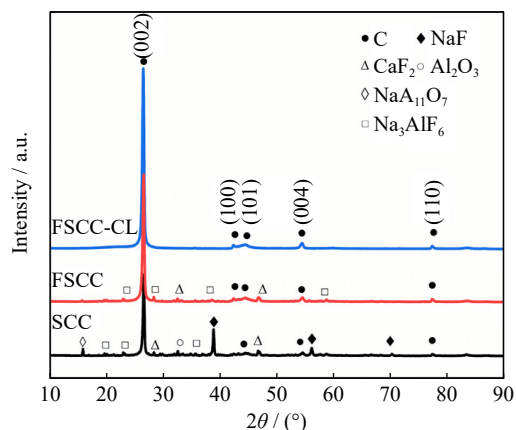


Fig. 4. XRD spectra of SCC, FSCC, and FSCC-CL.

Moreover, a large number of impurities were removed during the reaction process, which proves that FSCC-CL possessed a better graphite lamellar structure than SCC and FSCC.

The structural changes in SCC, FSCC, and FSCC-CL before and after the purification process were analyzed via Raman spectroscopy (Fig. 5). The Raman spectra of the three materials showed Raman wave numbers in the range of 1000 to 2000  $\text{cm}^{-1}$ . The two characteristic peaks were the D and G peaks located near 1350 and 1580  $\text{cm}^{-1}$ , which corresponded to a disordered band associated with amorphous carbon [19] and the vibration of  $\text{sp}^2$  carbon atoms within the carbon facets of the ordered graphite microcrystals [20], respectively. The FSCC-CL spectrum featured a sharper G peak, with a significantly higher peak intensity than those of the SCC and FSCC spectra. The FSCC-CL spectrum featured a weaker D peak than the SCC spectrum, suggesting that the carbon structure was gradually ordered during the impurity removal process and that a good graphite microchip layer structure was formed. Moreover, the D and G peak intensity ratio ( $I_D/I_G$ ) of SCC was 0.30, which is significantly higher than those of FSCC (0.14) and FSCC-CL (0.13). This indicates that the crystallinity of disordered carbon in SCC increased during the purification process, leading to an increase in the graphitization of the carbon materials.

The effects of the impurity removal process on the morphology of SCC, FSCC, and FSCC-CL were investigated via SEM (Fig. 6). Fig. 6(a)–(c) shows the SEM images and the

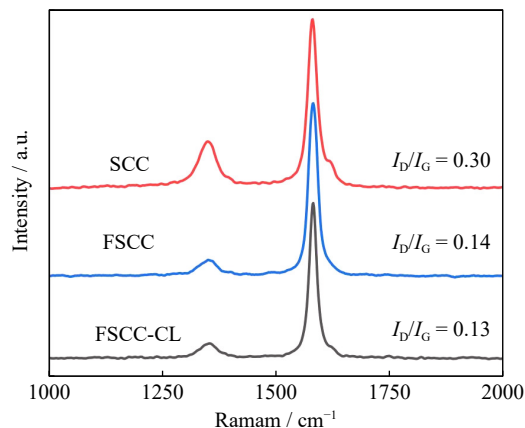


Fig. 5. Raman spectra of SCC, FSCC, and FSCC-CL.

mapping of the samples at magnifications of 10 and 2  $\mu\text{m}$ . SCC featured a rough surface with white non-carbonaceous particles, indicating the main form of impurities. After the flotation and acid leaching treatment, the dispersed white material disappeared, and the rich layered structure was gradually revealed. The mapping results showed that a large num-

ber of elements, such as F, Na, Ca, and Al, were removed during the purification process, while only C and some trace impurity elements remained. This also verifies the XRD results, indicating that a large number of impurities were removed. Additionally, the FSCC-CL lamellar structure became clearer owing to the removal of impurities.

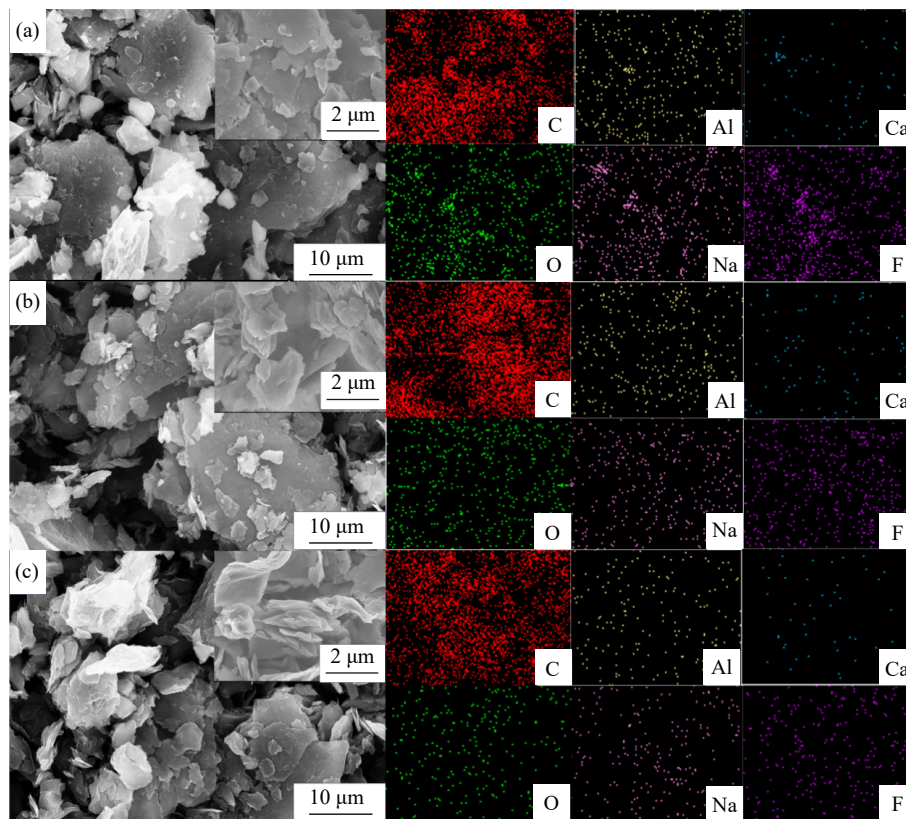


Fig. 6. SEM images and mapping images of SCC (a), FSCC (b), and FSCC-CL (c).

Fig. 7 shows the TEM results of FSCC-CL. Fig. 7(a)–(b) shows that after flotation–acid leaching purification and impurity removal, the FSCC-CL material exhibited a graphite flake layer structure with a large number of parallelly stacked graphite flakes. At higher resolution (Fig. 7(c)–(f)), an amorphous structure was visible in the FSCC-CL graphite crystals, owing to the presence of an amorphous carbon structure or closed pore defects formed through the chemical leaching method. This can also be verified through the electron diffraction from the selected area of the FSCC-CL, as shown in Fig. 7(f), with diffracted spots and diffracted halos [21]. According to the lattice streak image in Fig. 7(i)–(k), the lattice spacing of FSCC-CL was determined as 0.339 nm, which is slightly larger than that of graphite and thus conducive to lithium-ion migration [22].

### 3.4. Electrochemical characterization of FSCC-CL

To investigate the effect of the flotation–acid leaching method on the electrochemical properties of FSCC-CL, CV measurements were performed. The test was conducted for three cycles at the voltage range of 0.01–2.00 V and a scan rate of 0.1 mV/s. The CV curves of FSCC-CL after purification and decontamination presented a clear redox peak and a less distinct cathodic peak in the first cycle at 0.6–0.7 V

(Fig. 8(a)). The latter is attributable to asphalt embedded in the graphite in the SCC block surface, which resulted in the formation of an amorphous carbon solid electrolyte interface (SEI) coating [23], corresponding to irreversible capacity. However, this peak completely disappeared in the next two cycles, suggesting that a stable SEI was formed on the FSCC-CL surface in subsequent cycles [24–25]. The reduction peak near 0.1 V in the low-voltage scanning region indicates that  $\text{Li}^+$  was embedded in the graphite layer, and the oxidation peak at 0.3–0.4 V represented the de-embedding of  $\text{Li}^+$  from the graphite layer [26]. Furthermore, the CV curves overlapped in subsequent cycles, demonstrating the good reversibility and stability of FSCC-CL.

To investigate the electrochemical kinetic behavior of SCC, FSCC, and FSCC-CL before and after decontamination, electrochemical impedance spectroscopy (EIS) tests were conducted. Fitting was conducted using the Zview software [27]. The results are shown in Fig. 8(b), in which the small break corresponds to the solution impedance ( $R_f$ ). The Nyquist curves showed a semicircle in the mid/high-frequency range related to the SEI formed at the electrode surface ( $R_{\text{SEI}}$ ) and the charge-transfer impedance between the electrode and the electrolyte [28–30]. The Nyquist curves in the low-frequency region showed a diagonal line represent-

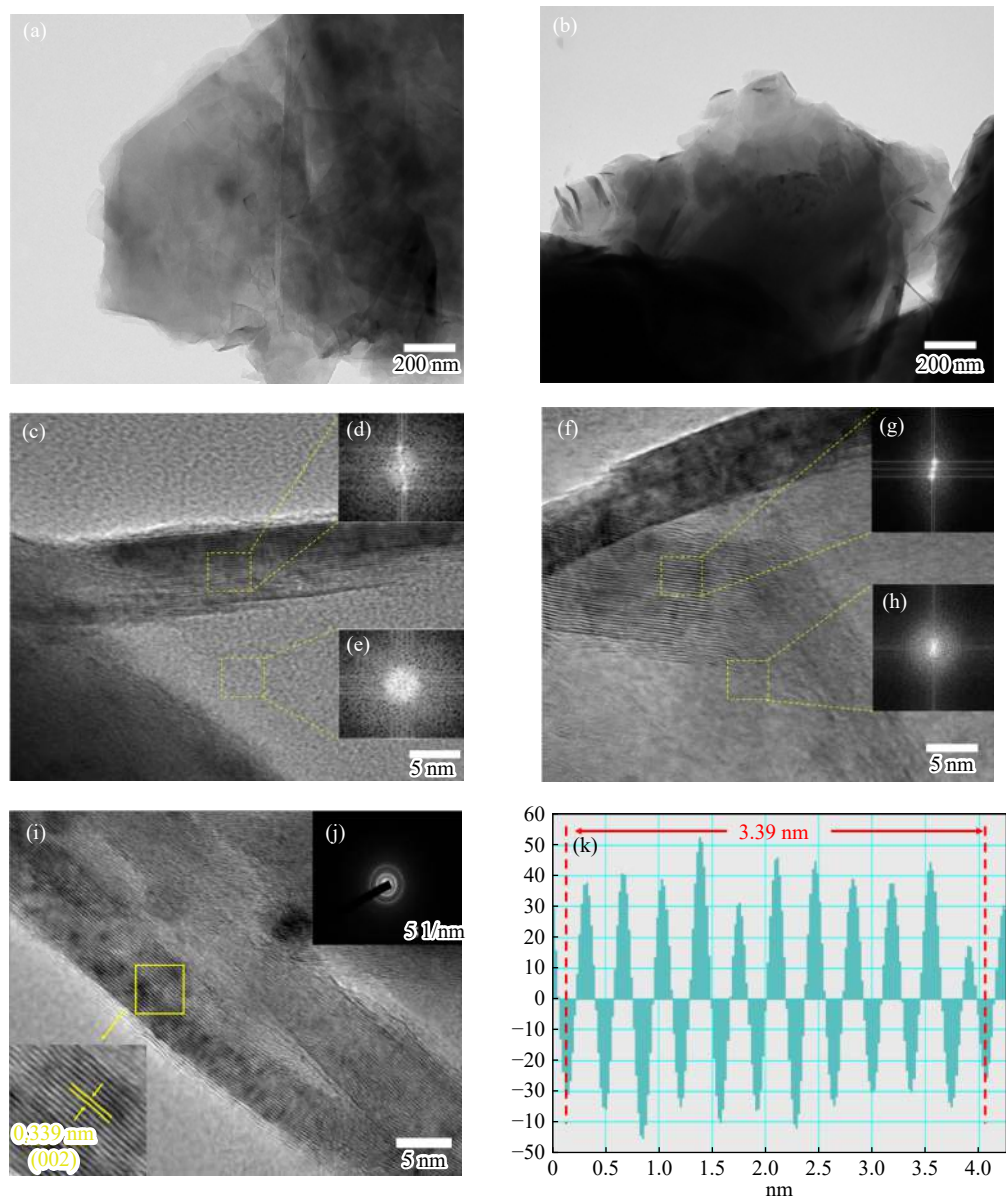


Fig. 7. TEM images (a–i), Fourier transform images (d, e, g, h), SAED results of FSCC-CL (j), and crystal lattice image (k).

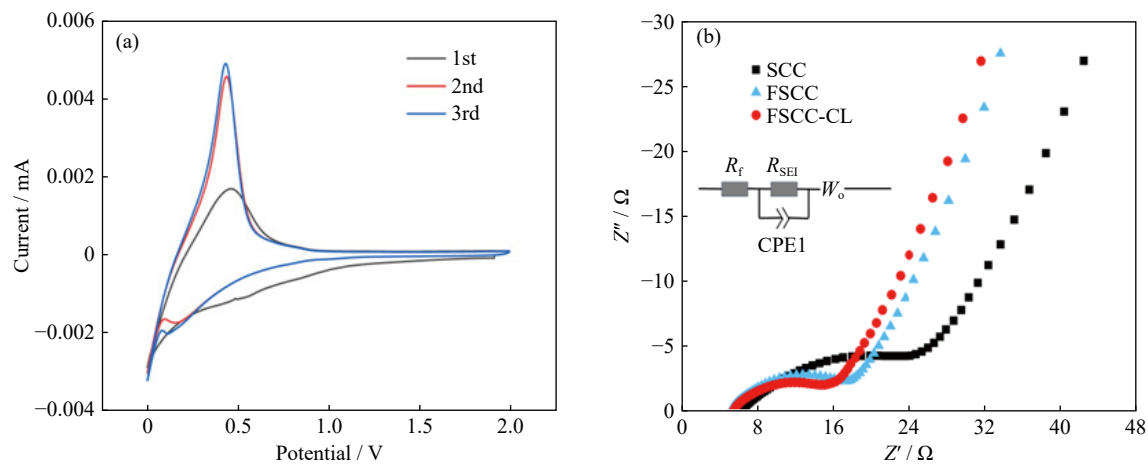


Fig. 8. CV curves (a) and electrochemical impedance spectra (b) of FSCC-CL.

ing the lithium solid-state diffusion within the active material ( $W_o$ ). According to the equivalent circuit diagram (Fig. 8(b)), the  $R_f$  and  $R_{SEI}$  of FSCC-CL were determined through fitting

as 3.01 and 5.73  $\Omega$ , respectively, which are smaller than those of FSCC (3.23 and 8.61  $\Omega$ ) and SCC (3.91 and 10.54  $\Omega$ ). Thus, the results showed that FSCC-CL exhibited the lowest



electrochemical impedance, high conductivity, and fast lithium-ion migration, thereby indicating that the internal resistance of the electrodes could be reduced through the flotation–acid leaching method.

Constant-current charge/discharge tests were performed on SCC, FSCC, FSCC-CL, and commercial graphite (Fig. 9(a)). At a current density of 0.1 C, the first-time charging capacities of SCC, FSCC, FSCC-CL, and commercial graphite were 242.3, 294.2, 348.2, and 353.1 mAh/g, respectively, and the charging capacities (and capacity retention) were maintained at 236.1 mAh/g (97.4%), 291.3 mAh/g (98.9%), 347.8 mAh/g (99.8%), and 351.7 mAh/g (98.3%), respectively, after 100 cycles. FSCC-CL exhibited a higher reversible capacity than FSCC and SCC after 100 cycles, attributable to the removal of impurities during the purification process. Moreover, the cycling curve and capacity retention rate of FSCC-CL remained stable with an increase in the number of cycles. Thus, FSCC-CL exhibited higher capacity retention than the other materials and good cycling ability, and its electrochemical performance was not inferior to that of commercial graphite.

To further compare the electrochemical rate capabilities of SCC, FSCC, FSCC-CL, and commercial graphite electrode materials, rate capability tests were performed at current densities of 0.1–2 C. As shown in Fig. 9(b), FSCC-CL

showed a higher capacity than the other three materials at each stage, with average specific capacities of 358.5, 347.1, 331.7, 252.9, and 146.2 mAh/g with the increase in the current density from 0.1 to 2 C. Notably, FSCC-CL achieved a higher specific capacity (408.1 mAh/g) than the initial specific capacity when the current density was restored to 0.1 C after 25 cycles. This is attributable to the successive embedding and de-embedding of lithium ions, which increased the spacing of the graphite layers and opened up more lithium-ion migration channels. Thus, subsequent lithium ions could be easily embedded into the material, resulting in capacity improvement [31]. The results showed that FSCC-CL had excellent reversibility and stability and demonstrated that the flotation–acid leaching process improved the rate capability of the electrode materials.

Fig. 10 shows the constant-current charge/discharge curves for the 1st and 50th cycles of SCC, FSCC, and FSCC-CL. Table 5 presents the first-cycle charge–discharge performance parameters of the three carbon materials and commercial graphite. Fig. 10(a) compares the charge–discharge curves of the SCC, FSCC, and FSCC-CL electrode materials. FSCC-CL exhibited the best performance, with a charging capacity of 348.2 mAh/g, a discharging capacity of 408.5 mAh/g, and a first-cycle coulombic efficiency of 85.3%. Additionally, FSCC-CL exhibited a longer voltage plateau than

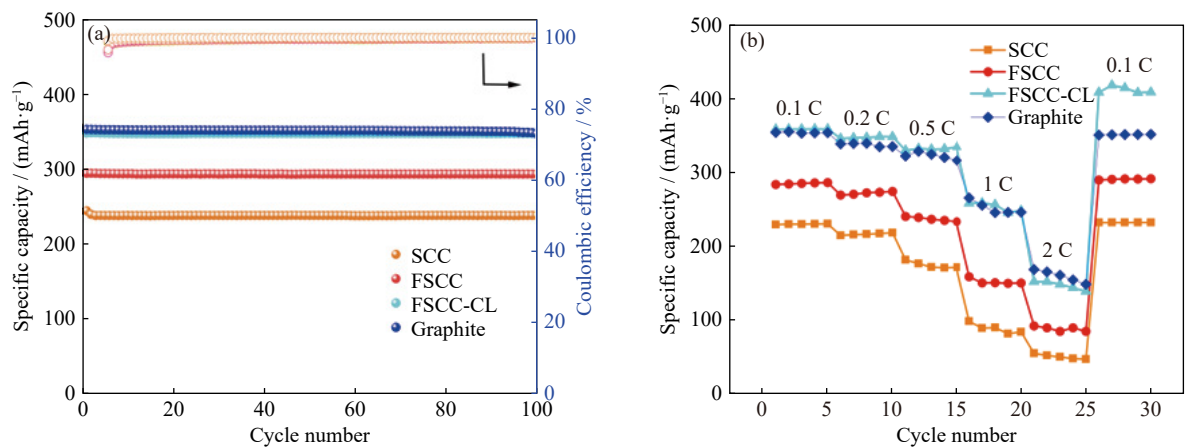


Fig. 9. Cycling performance at 0.1 C (a) and rate capabilities at different current densities (b) for SCC, FSCC, FSCC-CL, and graphite.

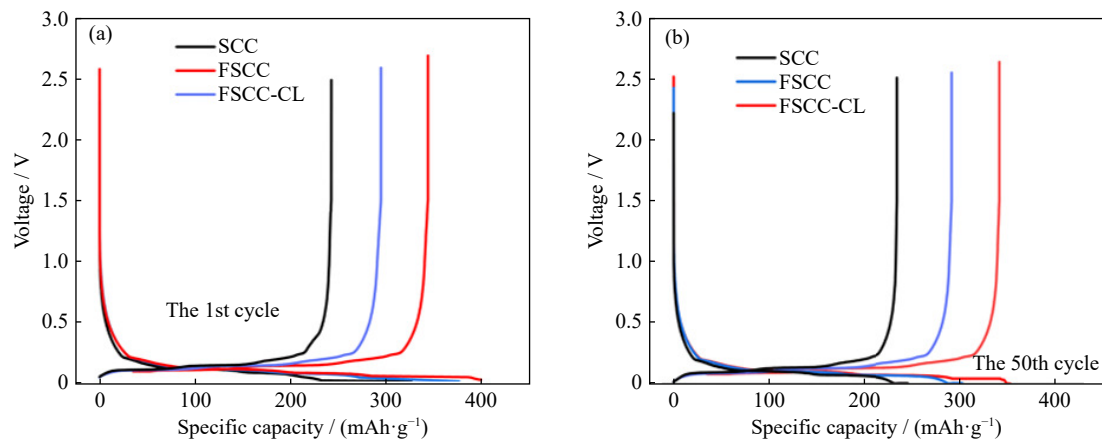


Fig. 10. Charge–discharge curves of SCC, FSCC, and FSCC-CL at the 1st cycle (a) and the 50th cycle (b).

**Table 5. Initial Coulombic efficiencies of graphite, SCC, FSCC, and FSCC-CL**

Sample	First charge specific capacity / (mAh·g <sup>-1</sup> )	First discharge specific capacity / (mAh·g <sup>-1</sup> )	Initial Coulombic efficiency / %
Graphite	353.1	415.1	85.1
SCC	242.3	325.0	74.5
FSCC	294.2	385.9	76.4
FSCC-CL	348.2	408.5	85.3

SCC and FSCC at voltages lower than 0.3 V. This corresponds to a reversible plateau of lithium ions embedded in the microcrystalline graphite interlayers, indicating that FSCC-CL formed oriented lamellar structures during the de-embedding process, consistent with a typical graphite lithium-ion storage mechanism. Additionally, the reversible specific capacity was further improved. The charging plateaus of the SCC, FSCC, and FSCC-CL electrodes after the 50th cycle exhibited similar characteristics to those observed in the first cycle (Fig. 10(b)). Moreover, the reversible capacity remained relatively stable with the increase in the number of cycles. The cycle retention rate was 99.9% after 50 cycles, demonstrating the excellent cycling stability of FSCC-CL.

## 4. Conclusion

The process of treating hazardous solid waste SCCs through a flotation–acid leaching process was proposed. Additionally, the obtained FSCC-CL material was demonstrated as a suitable lithium-ion battery anode material. Thus, this approach helps eliminate environmental pollution caused by SCCs and provides a practical carbon material resource. The impacts of the flotation and acid leaching processes on the materials were separately investigated through single-factor experiments. The results showed that the carbon content of SCC reached a maximum of 93wt% at a 90% proportion of –200-mesh flotation particle size, slurry concentration of 10wt%, rotation speed of 1600 r/min, and inflatable capacity of 0.2 m<sup>3</sup>/h. In the subsequent acid leaching process, the carbon content of SCC was 99.58wt% at an HCl concentration of 5 mol/L, leaching time of 100 min, leaching temperature of 85°C, and HCl/FSCC volume ratio of 5:1. Moreover, FSCC-CL showed a rich lamellar structure composed of graphitized carbon, with a large amount of amorphous carbon. The average carbon layer spacing of the graphitized carbon was 0.339 nm, which is slightly larger than the lamellar spacing of graphite and thus conducive to lithium-ion migration. In addition, FSCC-CL exhibited excellent electrochemical performance, with an initial capacity of 348.2 mAh/g at 0.1 C, a reversible capacity of 347.8 mAh/g after 100 cycles, and a cycling retention rate of 99.8%, thereby providing higher reversibility and cycling stability than commercial graphite. This study showed that SCCs have the potential to be used as anode materials, and this approach represents a viable pathway for the treatment and recycling of similar hazardous solid wastes.

## Acknowledgement

This study was supported by the National Natural Science

Foundation of China (No. 52274346).

## Conflict of Interest

Fengqin Liu is an editorial board member of this journal and was not involved in the editorial review or the decision to publish this article. We declare that they have no known competing financial interests or personal relationships that could have appeared to influence the work reported in this paper.

## References

- [1] J. Yuan, J. Xiao, F.C. Li, *et al.*, Co-treatment of spent cathode carbon in caustic and acid leaching process under ultrasonic assisted for preparation of SiC, *Ultrason. Sonochem.*, 41(2018), p. 608.
- [2] K. Yang, J. Li, W.L. Huang, *et al.*, A closed-circuit cycle process for recovery of carbon and valuable components from spent carbon cathode by hydrothermal acid-leaching method, *J. Environ. Manage.*, 318(2022), art. No. 115503.
- [3] M.Z. Xie, R.B. Li, H.L. Zhao, W. Liu, T.T. Lu, and F.Q. Liu, Detoxification of spent cathode carbon blocks from aluminum smelters by joint controlling temperature-vacuum process, *J. Cleaner Prod.*, 249(2020), art. No. 119370.
- [4] K. Yang, J. Li, C.P. Zhu, *et al.*, Separation and recovery of valuable elements from acid leachate of spent carbon cathode by fractional precipitation method, *J. Environ. Chem. Eng.*, 11(2023), No. 3, art. No. 110288.
- [5] Z. Zhu, L. Xu, Z.H. Han, *et al.*, Optimization of response surface methodology (RSM) for defluorination of spent carbon cathode (SCC) in fire-roasting aluminum electrolysis, *Miner. Eng.*, 182(2022), art. No. 107565.
- [6] Z. Yao, Q.F. Zhong, J. Xiao, S.C. Ye, L. Tang, and Z.H. Zhang, An environmental-friendly process for dissociating toxic substances and recovering valuable components from spent carbon cathode, *J. Hazard. Mater.*, 404(2021), art. No. 124120.
- [7] H.Y. Ren, C.L. Zhang, Q. Chang, H.M. Cheng, D.R. Li, and D.D. Zhang, Optimization of flotation conditions for spent pot lining carbon of aluminum reduction, *Light Met.*, (2017), No. 9, p. 26.
- [8] Z.N. Shi, W. Li, X.W. Hu, B.J. Ren, B.L. Gao, and Z.W. Wang, Recovery of carbon and cryolite from spent pot lining of aluminium reduction cells by chemical leaching, *Trans. Nonferrous Met. Soc. China*, 22(2012), No. 1, p. 222.
- [9] J. Xiao, J. Yuan, Z.L. Tian, *et al.*, Comparison of ultrasound-assisted and traditional caustic leaching of spent cathode carbon (SCC) from aluminum electrolysis, *Ultrason. Sonochem.*, 40(2018), p. 21.
- [10] B. Babu, P. Simon, and A. Balducci, Fast charging materials for high power applications, *Adv. Energy Mater.*, 10(2020), No. 29, art. No. 2001128.
- [11] G.Q. Yu, M.Z. Xie, Z.H. Zheng, Z.G. Wu, H.L. Zhao, and F.Q. Liu, Efficiently regenerating spent lithium battery graphite anode materials through heat treatment processes for impurity dissipation and crystal structure repair, *Resour. Conserv. Recycl.*,

- 199(2023), art. No. 107267.
- [12] K. Yang, Z.J. Zhao, X. Xin, Z.L. Tian, K. Peng, and Y.Q. Lai, Graphitic carbon materials extracted from spent carbon cathode of aluminium reduction cell as anodes for lithium ion batteries: Converting the hazardous wastes into value-added materials, *J. Taiwan Inst. Chem. Eng.*, 104(2019), p. 201.
- [13] K. Yang, P.Y. Gong, Z.L. Tian, Y.Q. Lai, and J. Li, Recycling spent carbon cathode by a roasting method and its application in Li-ion batteries anodes, *J. Cleaner Prod.*, 261(2020), art. No. 121090.
- [14] K. Yang, P.Y. Gong, Z.L. Tian, K. Peng, and Y.Q. Lai, Carbon recovered from spent carbon cathode of aluminum reduction cell towards its valorisation as negative electrodes for lithium ion batteries, *Diam. Relat. Mater.*, 109(2020), art. No. 108062.
- [15] K.Y. Shi, J. Wang, S.W. Wang, Z.M. Yu, P. Chen, and S. Li, Improving the flotation performance of coking coal using the reverse-direct flotation process, *Energy Sources Part A*, 40(2018), No. 23, p. 2886.
- [16] Ö. Öney, Optimization of operating parameters of graphite flotation circuit using box-behnken design, *Indian J. Chem. Technol.*, 25(2018), No. 2, p. 170.
- [17] F. Teng, T. Qu, and Y.N. Dai, Research of effect of alkali leaching factors on graphite purification through high pressure alkali leaching-atmospheric pressure acid leaching, *J. Kunming Univ. Sci. Technol. Nat. Sci. Ed.*, 41(2016), No. 1, p. 14.
- [18] B.L. Xing, C.T. Zhang, Y.J. Cao, *et al.*, Preparation of synthetic graphite from bituminous coal as anode materials for high performance lithium-ion batteries, *Fuel Process. Technol.*, 172(2018), p. 162.
- [19] G.X. Wang, X.P. Shen, B. Wang, J. Yao, and J. Park, Synthesis and characterisation of hydrophilic and organophilic graphene nanosheets, *Carbon*, 47(2009), No. 5, p. 1359.
- [20] Z.W. Yang, H.J. Guo, X.H. Li, *et al.*, Graphitic carbon balanced between high plateau capacity and high rate capability for lithium ion capacitors, *J. Mater. Chem. A*, 5(2017), No. 29, p. 15302.
- [21] S. Mancillas-Salas, J. Barroso-Flores, R. Villaurrutia, V. García-Montalvo, and E. López-Honorato, Production of few-layer graphene by wet media milling using organic solvents and different types of graphite, *Ceram. Int.*, 46(2020), No. 2, p. 2413.
- [22] Z. Ma, Y. Cui, X. Xiao, *et al.*, A reconstructed graphite-like carbon micro/nano-structure with higher capacity and comparative voltage plateau of graphite, *J. Mater. Chem. A*, 4(2016), No. 29, p. 11462.
- [23] Y. Gao, J.L. Zhang, Y.Q. Chen, and C.Y. Wang, Improvement of the electrochemical performance of spent graphite by asphalt coating, *Surf. Interfaces*, 24(2021), art. No. 101089.
- [24] J. Yang, X.Y. Zhou, Y.L. Zou, and J.J. Tang, A hierarchical porous carbon material for high power, lithium ion batteries, *Electrochim. Acta*, 56(2011), No. 24, p. 8576.
- [25] J.H. Hou, C.B. Cao, F. Idrees, and X.L. Ma, Hierarchical porous nitrogen-doped carbon nanosheets derived from silk for ultrahigh-capacity battery anodes and supercapacitors, *ACS Nano*, 9(2015), No. 3, p. 2556.
- [26] N. Cao, Y.L. Zhang, L.L. Chen, *et al.*, An innovative approach to recover anode from spent lithium-ion battery, *J. Power Sources*, 483(2021), art. No. 229163.
- [27] S. Zhang and P.F. Shi, Electrochemical impedance study of lithium intercalation into MCMB electrode in a gel electrolyte, *Electrochim. Acta*, 49(2004), No. 9-10, p. 1475.
- [28] Y.X. Chen, J. Li, Y.Q. Lai, J.M. Li, and Z.A. Zhang, Tailoring graphitic nanostructures in hard carbons as anode materials achieving efficient and ultrafast sodium storage, *J. Mater. Sci.*, 53(2018), No. 14, p. 10313.
- [29] J.K. Ou, Y.Z. Zhang, L. Chen, *et al.*, Nitrogen-rich porous carbon derived from biomass as a high performance anode material for lithium ion batteries, *J. Mater. Chem. A*, 3(2015), No. 12, p. 6534.
- [30] S.B. Yang, X.L. Feng, L.J. Zhi, Q. Cao, J. Maier, and K. Müllen, Nanographene-constructed hollow carbon spheres and their favorable electroactivity with respect to lithium storage, *Adv. Mater.*, 22(2010), No. 7, p. 838.
- [31] A. Ramos, I. Cameán, N. Cuesta, and A.B. García, Graphitized stacked-cup carbon nanofibers as anode materials for lithium-ion batteries, *Electrochim. Acta*, 146(2014), p. 769.